The Cryosphere Discuss., 7, 709–741, 2013
www.the-cryosphere-discuss.net/7/709/2013/
doi:10.5194/tcd-7-709-2013

The Cryosphere Discussions
Open Access

Snowdrift modelling for Vestfonna ice cap, north-eastern Svalbard

T. Sauter[1], M. Möller[1], R. Finkelnburg[2], M. Grabiec[3], D. Scherer[2], and C. Schneider[1]

[1]Department of Geography, RWTH Aachen University, Germany
[2]Department of Ecology, Technische Universität Berlin, Germany
[3]Department of Geomorphology, University of Silesia, Poland

Received: 5 February 2013 – Accepted: 14 February 2013 – Published: 28 February 2013

Correspondence to: T. Sauter (tobias.sauter@geo.rwth-aachen.de)

Published by Copernicus Publications on behalf of the European Geosciences Union.

Abstract

The redistribution of snow by drifting and blowing snow frequently leads to an inhomogeneous snow mass distribution on larger ice caps. Together with the thermodynamic impact of drifting snow sublimation on the lower atmospheric boundary layer, these processes affect the glacier surface mass balance. This study provides a first quantification of snowdrift and sublimation of blowing and drifting snow on Vestfonna ice cap (Svalbard) by using the specifically designed "snow2blow" snowdrift model. The model is forced by atmospheric fields from the Weather Research and Forecasting model and resolves processes on a spatial resolution of 250 m. Comparison with radio-echo soundings and snow-pit measurements show that important local scale processes are resolved by the model and the overall snow accumulation pattern is reproduced. The findings indicate that there is a significant redistribution of snow mass from the interior of the ice cap to the surrounding areas and ice slopes. Drifting snow sublimation of suspended snow is found to be stronger during winter. It is concluded that both processes are strong enough to have a significant impact on glacier mass balance.

1 Introduction

In high arctic regions, redistribution of snow mass by wind drift has an important impact on the balance of glaciers. The intensity of the redistribution process is essentially given by the interaction of the inherent erosional capacity of the wind flow and the snow pack characteristics. Particularly along the margin of larger ice caps, persistent katabatic winds become often strong enough to effectively remove snow from the surface and re-accumulate the eroded snow mass within the surrounding areas (e.g. Boon et al., 2010; Mernild et al., 2006). Once snow particles become mobile, they can be advected over long distances by the mean flow, while influencing the turbulent structure of the atmospheric boundary layer. Snow particles, which are entrained far upwards (above 2 m) by turbulent eddies are generally refered to as blowing snow, whereas

TCD
7, 709–741, 2013

the advection of snow mass within the surface layer is termed drifting snow. During transport part of the snow mass is removed by sublimation which modifies the vertical temperature and moisture profiles of the near-surface layer. The cooler and more humid air masses, then have a non-neglectable impact on the surface energy fluxes. Since the effect on mass balance can be strong, bridging the gap between drifting and blowing snow and the local scale impact on glacier mass balance in polar regions has been addressed by several glaciological studies (e.g. Jaedicke, 2002; Bintanja, 1998; Lenaerts et al., 2010, 2012).

The importance of drifting and blowing snow in the European Arctic has early been postulated by Ahlmann (1933). Based on point field measurements in Nordaustlandet, he estimated that at least 1/8 of the total snow accumulation is redistributed by wind. The first detailed accumulation map of Nordaustlandet (Spitsbergen) has been provided by Schytt (1964), based on point measurements collected during the Swedish Glaciological Expedition in 1957/58. Later, better insights along several transects have been gained by extensive repeated ground penetrating radar measurements carried out by Taurisano et al. (2007) and Grabiec et al. (2011). Both studies substantially contributed to a better understanding and a consistent idea of the spatial snow cover pattern on the two large ice caps on Nordaustlandet, Austfonna and Vestfonna. Their findings have been recently affirmed by on-site snow measurements from Möller et al. (2011b) and Beaudon et al. (2011). Unfortunately, due to the heterogeneity of the complex snowdrift processes a comprehensive, glacier wide spatio-temporal quantification by measurements, however, proof to be a challenging task.

This study presents the first spatio-temporal estimate of snowdrift in the southwest part of Vestfonna ice cap. We discuss the processes involved and describe the mathematical framework of the specifically designed three-dimensional *snow2blow* model. The model is then applied to Vestfonna ice for the accumulation period 2008/2009. Model results are compared with radio-echo sounding measurements and on-site snow-pitdata. Finally, the contribution and influence of individual component on the snow distribution is discussed in detail.

TCD
7, 709–741, 2013

2 Study area

The ice cap Vestfonna covers a surface area of 2340 km^2 in 2005 (Braun et al., 2011) and is thus the second largest single ice mass of the Svalbard archipelago and among the largest ice caps of the Eurasian Arctic (see Fig. 1). Its star-shaped ice dome is formed by an east-west oriented ridge that extends over the main summit, Ahlmann Summit. From the eastern summit, which is the highest point of the ice cap (647 m over WGS84 ellipsoid, Braun et al., 2011), a secondary ridge extends towards the north. Apart from these main ridges the morphology of Vestfonna is dominated by several land-terminating ice lobes and extensive outlet glacier basins that form marine terminating, calving glacier fronts.

The strongly maritime climate of Svalbard is characterized by the contrasting influences of warm and humid North Atlantic air masses to the south and cold and dry Arctic air masses to the northeast (Svendsen et al., 2002). The warm West Spitsbergen Current (Walczowski and Piechura, 2011) frequently causes sea ice-free conditions along the western part of the archipelago while the eastern areas are directly influenced by cold Arctic ocean currents (Loeng, 1991) with closed sea-ice cover during most winters. Extratropical cyclones mainly control the synoptic-scale variability in the southern parts of the archipelago while the Arctic high pressure system forms the strongest influencing factor for the northern parts (Skeie, 2000). The synoptic forcing markedly imprints on the surface climate especially during the winter months (Bednorz and Fortuniak, 2011). The synoptic-scale airflow across the archipelago is dominated by southerly directions during the summer season while during winter northeasterly directions prevail (Käsmacher and Schneider, 2011).

Due to its location within the archipelago, Nordaustlandet is less directly influenced by the warmer Atlantic air and water masses. Its climatic setting is mainly governed by easterly weather systems originating in the Barents Sea region (Taurisano et al., 2007). These provide the major moisture source for precipitation during the winter season (Førland et al., 1997) with the absolute amounts partly depending on sea-ice coverage

TCD
7, 709–741, 2013

(Rogers et al., 2001). During conditions of easterly air flow, Vestfonna is located in the lee of its larger and higher neighbour Austfonna which makes precipitation sums being generally smaller here (Hagen, 1993).

Snow accumulation throughout the slopes of Vestfonna was found to be mainly governed by terrain elevation (Möller et al., 2011a,b). Along the main ridges the pattern of accumulated winter snow shows substantial zonal variability that differs between individual years (Beaudon et al., 2011). The prevalence of katabatic wind directions throughout the slopes of the ice cap (Claremar et al., 2012) promotes radial drifting snow trajectories while synoptic winds and thus less consistent drifting snow directions dominate on the ridges (Möller, 2012; Möller et al., 2013). Overall, the magnitude of snow accumulation across the ice cap shows high interannual variability and therewith reflects the synoptic forcing (Beaudon et al., 2011).

3 Field observations

The here presented study requires different types of field data for validation purposes, i.e. snow-depth information from radio-echo sounding and snow-pit analysis as well as in situ meteorological measurements at automatic weather stations.

A snow-depth profile that is acquired from radio-echo sounding carried out in spring 2009 by Grabiec et al. (2011) serves as a basis for the validation of the modelled snow accumulation pattern (Fig. 1). The first part of this profile that is used in this study extends over 14 km and reaches from the forefield of the northwestern land-terminating parts of Vestfonna up to the main ridge of the ice cap and further on to Ahlmann Summit. The second used part of the profile covers 32 km of the western part of the main ridge. The original snow-depth soundings provide point data that are unevenly distributed along the profile line. For application in model validation we smoothed the original data using a 21-point moving-window filter in order to eliminate local outliers. Afterwards the smoothed profile data were averaged to fit the 250 m pixel resolution of the modelling domain. Snow depth along the profile ranges between 0 and 2.24 m.

TCD
7, 709–741, 2013

According to the measurements three different types of altitude dependent accumulation patterns are observable, i.e. inversion, precipitation and redistribution. At elevations below 350 m the snow accumulates in a permanent aggregation wedge (Grabiec et al., 2011; Ahlmann, 1933) and forms a surrounding snow band that is clearly visible on satellite images throughout the entire year. Within a small zone of this snow band snow depth gradually decreases with increasing altitude. In contrast, snow depth above an altitude of 350 m tends to increase with altitude. Throughout the uppermost parts of the ice cap the spatial distribution of snow depth is mainly determined by snowdrift that result in frequent sastrugi formation and thus in a high local-scale variability of snow accumulation. The radar measurements shown in Figs. 2 and 3 indicate both low and high frequency fluctuations of snow depth that can be attributed to short and longwave sastrugi formation as it is especially visible between markers D and E.

Point related, multi-year snow-cover data from an extensive snow-pit study (Möller et al., 2011b) provide information on snow depth and density for 21 points on Vestfonna and nearby De Geerfonna for the period 2007–2010. According to this study, the mean density of the snow pack lies in the range 300–400 $\mathrm{kg\,m^{-3}}$. The snow-pit data are integrated in the discussion of qualitative model performance with respect to interannual persistence of the ice cap-wide snow-depth pattern.

Meteorological data from an automatic weather station operated on the northwestern slope of Vestfonna (VF-AWS, Fig. 1) since spring 2008 is used for validation of WRF derived fields of wind speed and direction, air temperature and relative humidity. The records used here comprise the period September 2008 to May 2009.

4 Physical processes in two-phase flow

The redistribution of snow strongly depends on the available turbulent kinetic energy of the atmospheric boundary layer, and thus from the momentum flux and the surface shear effects (Liston and Sturm, 1998; Lehning et al., 2008; Bintanja, 2000). Once the surface shear stress exceeds the inertia and the cohesive bonds of the snow particles,

TCD
7, 709–741, 2013

transport takes place. Within a thin surface layer the ejected particles follow a ballistic trajectory under the influence of gravity. The rebounds of these particles on the snow surface, again, are able to eject more grains. This near-surface layer is barely influenced by turbulence so that the prevailing particle transport mechanism is pure saltation. Depending on the momentum flux some of the particles within the saltation layer may be entrained further upwards against their gravitative force by turbulent diffusion and further suspended by the mean flow. Once the particle is in suspension the particle velocity is assumed to be equivalent to the fluid velocity.

Blowing and drifting of snow is considered to be a dilute two-phase flow consisting of solid snow particles in a fluid phase. Transport- and exchange processes in such two-phase flows are given by turbulent fluid motion, which in turn is affected by the presence of the particles. Thus, snow particle can either enhance or damp turbulent velocity fluctuations depending on the different characteristic time and length scales of the flow. It appears that, if snow particles are small compared to the turbulent length scale they tend to absorb turbulent kinetic energy (Gore and Crowe, 1989). The evolution of turbulence in the presence of snow particles is a function of the Stokes number St, which is given by the ratio of the particle relaxation time and the characteristic time scale of energy containing eddies (Kolmogorov time scale $\tau = (\nu/\epsilon)^{1/2}$). Assuming that the particle diameters of drifting snow is typically in the range 10–400 µm and the Kolmogorov length scale of the atmosphere is $(\eta = (\nu^3/\epsilon)^{1/4})$ $\eta \approx 1$ mm leads to a St < 1. Such a small Stokes number implies that the particles enhance the dissipation of turbulent energy in order to keep the particles in suspension. This reduces the available turbulent energy for further entrainment.

Elgobashi (1994) likewise described interaction effects of particle-laden flows by the Stokes number St and the average volumetric particle concentration. Since the average volumetric snow particle concentration of suspended snow is usually below 10^{-3} (Bintanja, 2000; Gauer, 2001; Schneiderbauer et al., 2008), and thus the average distance between the particles is large compared to their size, it is feasible to neglect interaction effects (Crowe et al., 1996; Elgobashi, 1994). As shown by Bintanja (2000)

TCD
7, 709–741, 2013

the presence of particles also modifies the mean wind velocity profile. Snow particles in suspension are balanced by the particle-fluid drag force and the counteracting gravity force. If this equilibrium is perturbed by turbulent motion the air parcel experience an anomalous buoyancy, which is similar to a thermally stable turbulent layer. As a consequence of the stable stratification the density of the fluid-particle mixture increases towards the surface. Therefore, friction velocity u_* is not constant with height according to $u_* = \sqrt{\tau_0/\rho}$, leading to a reduction of the turbulent exchange coefficient $K_M = \kappa u_* z$. Due to the change of the turbulent exchange coefficient the wind speed gradient, and thus the wind speed increases.

5 Model description

5.1 General comments and model setup

Snow erosion and transport processes are inherently linked to the characteristics of the air flow and snow properties. Therefore, the quantitative assessment of snow redistribution requires an approximation of the buoyant, turbulent surface wind field. Similar to previous studies (e.g. Liston and Sturm, 1998; Naaim et al., 1998; Schneiderbauer et al., 2008; Bintanja, 2000; Pomeroy and Gray, 1990; Gauer, 2001; Durand et al., 2005), the interactions between particles are neglected and snow particles are treated as a continuous phase solely interacting with the background flow. The proposed model solves the Reynolds averaged Navier–Stokes equation using the k-ω turbulence model. The model is implemented within the open source C++ library OpenFOAM and is freely downloadable at the author's webpage.

TCD
7, 709–741, 2013

5.2 Governing equations

The turbulent flow is assumed to be incompressible, so that the continuous continuity equation reduces to

$$\frac{\partial u_i}{\partial x_i} = 0 \tag{1}$$

Taken the particle buoyancy and Boussinesq approximation into account while neglecting the Coriolis force, the extended momentum equation can be written using Einstein's summation notation as

$$\frac{\mathrm{d}u_i}{\mathrm{d}t} = -\frac{1}{\rho}\frac{\partial p}{\partial x_i} - \delta_{i3}g + \nu_t \frac{\partial^2 u_i}{\partial x_j^2} - g\delta_{i3}\frac{\phi_s}{\rho} + \delta_{i3}g\left[1 - \beta(\bar{\theta} - \theta_0)\right] \tag{2}$$

where x_i ($i = 1,2,3$) are the Cartesian coordinates and u_i are the Cartesian components of the velocity vector. The fourth term on the right side describes the particle buoyancy. The Boussinesq approximation $g[1 - \beta(\bar{\theta} - \theta_0)]$ considers density changes due to temperature variations in the lower atmosphere and primarily forces the katabatic surface winds. The β is the coefficient of thermal expansion. All remaining terms are similar to the common Navier–Stokes equation (e.g. Stull, 1988). Proceeding from the instantaneous internal energy equation the conservation equation of the potential temperature can be derived, and finally becomes

$$\frac{\partial \bar{\theta}}{\partial t} + \frac{\partial(\bar{\theta}u_i)}{\partial x_i} - \frac{\partial}{\partial x_j}\left(\kappa_{\mathrm{eff}}\frac{\partial \bar{\theta}}{\partial x_j}\right) = 0 \tag{3}$$

whereas temperature changes by radiative forcing and phase change of water are neglected in this study. The Reynolds averaged momentum equation is closed using the k-ω turbulence model. The equation for the turbulent kinetic energy, k, reads as

$$\frac{\partial k}{\partial t} + \frac{\partial u_j k}{\partial x_j} = P_k - \beta_k^* k\omega + \frac{\partial}{\partial x_j}\left[\left(\nu + \frac{\nu_t}{\sigma_k^*}\right)\frac{\partial \omega}{\partial x_j}\right] \tag{4}$$

TCD
7, 709–741, 2013

with the production rate of kinetic energy by the mean velocity field, P_k, given by

$$P_k = \nu_t \left(\frac{\partial u_i}{\partial x_j} + \frac{\partial u_j}{\partial x_i} \right) \frac{\partial u_i}{\partial x_j} \tag{5}$$

The equation for dissipation uses the inverse time scale ω that determines the scale of turbulence

$$\frac{\partial \omega}{\partial t} + \frac{\partial u_j \omega}{\partial x_j} = \alpha \frac{\omega}{k} P_k - \beta_k \omega^2 + \frac{\partial}{\partial x_j} \left[\left(\nu + \frac{\nu_t}{\sigma^*_\omega} \right) \frac{\partial \omega}{\partial x_j} \right] \tag{6}$$

Based on these equations the turbulent viscosity is defined as

$$\nu_t = \frac{k}{\omega} \tag{7}$$

While the particle effect on turbulence stability is taken into account (see Eq. 2) we neglect the enhanced dissipation of turbulent kinetic energy by snow particles, even though this effect is present.

The rate of snow mass change $\partial \phi_s / \partial t$ is described by the continuum equation for conservation of mass

$$\underbrace{\frac{\partial \phi_s}{\partial t}}_{\text{(I)}} + \underbrace{\frac{\partial (\phi_s u_i)}{\partial x_i}}_{\text{(II)}} = \underbrace{\frac{\partial}{\partial x_3} \left(K_M \frac{\partial \phi_s}{\partial x_3} - V \phi \right)}_{\text{(III)}} + \underbrace{\left(\frac{\partial \phi_s}{\partial t} \right)_{\text{sub}}}_{\text{(IV)}} \tag{8}$$

Since we make the simplifying assumption that the relative velocity between the two phases is always zero there is no need to use a combined phase continuity equation as it reduces to the equivalent single phase flow equation. The drifting snow flux in the i direction is $\phi_s u_i$ and therefore the net flux due to the fluid motion is given by the divergence of the mass flux (Term II). Term IV gives the mass loss of suspended snow

TCD
7, 709–741, 2013

by sublimation. Besides the vertical entrainment of snow particles by turbulent diffusion, there is a downward flux $-V\phi$ due to gravity (Term III). For the sake of simplicity the terminal fallout velocity V is assumed to be constant. The total amount of drifting and blowing snow mass depends on the erosion flux and accumulation flux, respectively, which are discussed in detail in the next section.

5.3 Erosion and accumulation flux

The snow mass within the saltation layer primarily gains by the aerodynamic entrainment of snow particles from the underlying snowpack. According to Anderson and Haff (1991) the erosional mass flux q_e is assumed to be proportional to the excess surface shear stress

$$q_e = e_{salt}\left(\rho u_*^2 - \rho_a\, u_{th}^2\right) \tag{9}$$

Once the surface shear stress u_*^2 exceeds the friction threshold velocity u_{th} particles are ejected from the snowpack. The efficiency of the erosional process is described by the e_{salt}. The friction threshold velocity strongly depends on the physical properties of the snowpack. Through the process of kinetic and melt-freeze metamorphosis the snowpack is in a constant state of change. Both processes modify the snow density and hence the kinetic resistance of the snowpack. The friction threshold velocity is therefore assumed to be proportional to the snow density,

$$u_{th} = 0.0195 + \left(0.021\sqrt{\rho_s}\right) \tag{10}$$

Typical values for u_{th} are in the range of $0.3\,m\,s^{-1}$ for loose fresh snow to $0.6\,m\,s^{-1}$ for consolidated firn. Based on these values saltation starts at wind speed u_{10} of about 7–$14\,m\,s^{-1}$ for consolidated snow and of about 4–$11\,m\,s^{-1}$ for fresh snow (cf. Pomeroy and Gray, 1990). However, the ejected particles do have a strong impact on the prevailing flow which affects the mass exchange process. The force exerted by the particles on

TCD
7, 709–741, 2013

the wind field lowers the wind shear stress and consequently reduces the capacity to eject further particles. To allow for such effect the friction velocity is corrected by the particle-saturation ratio (Naaim et al., 1998). Taking into account the particle-saturation ratio the corrected friction velocity u_*^{corr} can be written as

$$u_*^{\mathrm{corr}} = u_* + (u_{\mathrm{th}} - u_*)\left(\frac{\phi_{\mathrm{s}}}{\phi_{\mathrm{max}}}\right)^2 \tag{11}$$

If the drifting snow density reaches saturation ϕ_{max} the friction velocity reduces to the friction threshold velocity and entrainment is suppressed. In case the saltation layer contains no particles both, the corrected and uncorrected, friction velocity are equal. The maximum concentration ϕ_{max} is estimated by the following semi-empirical relationship (Pomeroy and Male, 1992),

$$\phi_{\mathrm{max}} = \frac{\rho}{3.29 u_*}\left(1 - \frac{u_{\mathrm{th}}^2}{u_*^2}\right) \tag{12}$$

By replacing u_* by u_*^{corr} in Eq. (9), the final erosion flux

$$q_{\mathrm{e}} = e_{\mathrm{salt}}\left(\rho\left[(u_{\mathrm{th}} - u_*)\left(\frac{\phi_{\mathrm{s}}}{\phi_{\mathrm{max}}}\right)^2 + u_*\right]^2 - \rho u_{\mathrm{th}}^2\right) \tag{13}$$

is obtained. Once the threshold velocity exceeds the friction velocity deposition is possible. Similar to Beyers et al. (2004) the deposition flux is simply related to the downward flux (Eq. 8) and the shear stress ratio.

$$q_{\mathrm{d}} = V\phi \cdot \max\left(\frac{u_{\mathrm{th}}^2 - u_*^2}{u_{\mathrm{th}}^2}, 0\right) \tag{14}$$

TCD
7, 709–741, 2013

5.4 Sublimation

Sublimation of suspended snow particles is an important process, particularly in arctic regions where saturation deficits are usually large. The used approach approximates the sublimation loss rates by

$$q_s = \psi_s \phi_s h_* + \int_{h_*}^{z} \psi_t(z)\phi_t(z)\mathrm{d}z \quad (15)$$

where the subscripts s and t indicate the saltation (with height h_*) and suspension layer, respectively. The sublimation-loss-rate coefficients, ψ_s and ψ_t, represent the time rate of change of snow particle mass as a function of the mean particle size, solar radiation, saturation deficit and conductive and advective energy and moisture transfer. For a detailed description see Schmidt (1972, 1991), Pomeroy and Gray (1995), Pomeroy et al. (1993), Bintanja (2000) and Naaim et al. (1998). The effect of sublimation on the vertical profiles of temperature and humidity is not included in this work. This simplified assumption ignores the fact that sublimation of drifting snow is a self-limiting process, in the sense that the intensity depends on the saturation deficit of the environment. Neglecting the feedback mechanism on the atmospheric profiles can therefore lead to an overestimation of snow drift sublimation.

6 Numerical setup

The snow2blow model is applied to the southwestern part of Vestfonna (79°41′49.029″ N to 80°04′09.647″ N and 18°12′33.253″ W to 19°58′17.844″ E) with an horizontal resolution of 250 m. For this study the domain top is set to 3000 m consisting of 5 vertical layers within in the near surface layer (5 m), and further 40 vertical layers above. This setup allows for a better representation of the turbulent near-surface

TCD
7, 709–741, 2013

wind field and the derived fluxes therefrom. The decision to highly resolve the surface layer was done at the expense of the horizontal domain size, because any additional vertical layer increases the computational cost exponentially. The daily atmospheric fields from the WRF with a horizontal resolution of 2 km are mapped onto the snow2blow grid. It is then forced by the lateral boundaries of the WRF, so that an independent internal turbulent wind field can evolve. The snow mass flux at the boundaries for the saltation layer is given by the formulation of Pomeroy and Gray (1990)

$$q_{\text{salt}} = \frac{0.68\rho}{u_* g} u_{\text{th}} \left(u_*^2 - u_{\text{th}}^2\right) \tag{16}$$

The inlet snow density profile for the suspension layer is given by Pomeroy and Male (1992)

$$\phi_{\text{s}}(u_*, z) = 0.8 \cdot \exp\left[-1.55\left(4.784 u_*^{-0.544} - z^{-0.544}\right)\right] \tag{17}$$

Up to now, no parametrization scheme for the snow cover evolution is included, which might account for the snow densification processes. However, in order to prevent that the entire snow cover is eroded at once only the present day fresh snow is allowed to redistribute. This is an acceptable assumption given the fact, that the high wind velocities lead to a rapid densification of the upper snow cover (Möller et al., 2011b) and formation of sastrugi. Snowdrift model parameters used for the simulations are given in Table 2.

The daily atmospheric fields employed by the WRF are based on the six hourly Global Forecast System (GSF) global gridded analysis of the National Centers for Environmental Prediction (NCEP) with a spatial resolution of 1.0°. The original fields of this product are reprocessed and dynamically downscaled to one day temporal and 2 km spatial resolution using a polar-optimized version of the WRF model (PWRF 3.1.1). Lateral boundary conditions for the downscaling are given by NCEP low resolution Real Time Global sea-surface temperature analysis (NCEP RTG SST) with a spatial resolution of 0.5° and Advanced Microwave Scanning Radiometer EOS (AMSR-E) daily sea

TCD
7, 709–741, 2013

ice concentrations with a spatial resolution of 12.5 km. The static geographical fields of the WRF model are initialized using the United States Geological Survey (USGS) standard data sets. The applied downscaling procedure features a telescope two-way nesting of three polar stereographic domains (30, 10 and 2 km horizontal resolution). The inner domain of this nesting is used as input to the snow2blow model. All three domains are resolved in 28 vertical layers reaching up to the 50 hPa level. The temporal reprocessing from the original six hourly to the final daily datasets is done using the method presented by Maussion et al. (2010). The setup of the physical parameterizations of the WRF model is motivated by Hines et al. (2011) and Hines and Bromwich (2008).

7 Results and discussion

7.1 WRF model evaluation

The performance of the WRF generated atmospheric fields was evaluated with data from the VF-AWS. Figure 4 shows the observed wind conditions at the VF-AWS and the closest WRF grid point, respectively. Frequent strong winds of up to 15 $m s^{-1}$ are observed from the south-easterly direction, clearly indicating the persistent katabatic wind flows. In contrast, the more fluctuating north-westerly flows are weak during the entire observation period. For validation the best out of the four closest WRF model grids points was chosen and compared with the observations (Claremar et al., 2012). The WRF wind speed at 10 m height was corrected to the corresponding sensor height at 2.4 m using Monin-Obukhov theory for stable boundary layer (Stull, 1988), while the Obukhov length has been derived from the WRF output variables. The model slightly overestimates the katabatic wind speeds and tends to have a more southerly wind component (Fig. 4). Air temperatures at 2 m height varied at the VF-AWS between −37.9 and +5.8 °C during this period. Observed and modelled air temperatures significantly correlate with an r^2 = 0.98, but show a neglectable cold bias of −0.05 K, which is

TCD
7, 709–741, 2013

a problem of the WRF model that was previously reported for the study region (Claremar et al., 2012).

Figure 5 shows the spatial distribution of the uncorrected snow water equivalent (SWE) field for the accumulation period September 2008 to May 2009 obtained from the WRF model run. Snow distribution is predominantly controlled by altitude ranging from 0.2 m w.e. in coastal areas to 0.6 m w.e. in higher regions along the ice cap ridge. The general increase of SWE with altitude is consistent with studies carried out by Grabiec et al. (2011) and Möller et al. (2011b). However, these studies also emphasize that drifting and blowing snow often lead to local scale deviation from this dominant pattern.

7.2 Snowdrift

The modelled distribution of SWE on Vestfonna ice cap for the period September 2008 to May 2009 is shown in Fig. 6. Snow is heterogeneously distributed across the domain ranging between 0.11 m w.e. in the southeast and 0.49 m w.e. in higher regions. This corresponds to a total snow loss of ∼ 10–20 % along the ridge by blowing snow. At the ice cap slopes the total snow loss is about 5–15 %. Parts of the eroded and suspended snow mass is later accumulated in the undulating northwestern forefield of the ice cap. In regions of disturbed flow, re-accumulation can be more than 0.1 m w.e. for this period. In this way, the De Geerfonna ice body receives between 15 and 20 % of its total snow mass by drifting snow which therefore is an important term for the local mass balance. Snow mass blowing away from the ice cap to the open sea was not quantified in this study. Jaedicke (2002) estimated that snow mass loss to the open sea only accounts for 0.2 % of the precipitated mass in Svalbard. In most areas near the ice fringe and the western forefield accumulation and erosion are widely balanced. In contrary, largest snow mass losses of 0.10–0.25 m w.e. (30–50 %) are found southeasterly of the main ridge. A comparison of modelled snow depths with radio-echo soundings and snow pits shows that there is a bias of +0.07 m w.e. along the ridge, while at the De Geerfonna snow is underestimated by about −0.08 m w.e. by the model.

TCD
7, 709–741, 2013

However, these errors are insignificant in the light of the spatial variability of snow depth, which sometimes may vary between ±0.13 m w.e. within very short distances of less than 50 m caused by sastrugi formation. Due to the limited information on the spatial distribution it, however, remains uncertain, whether the deviations represent a systematic pattern or are purely random.

The occurrence of drifting and blowing snow events follow a pattern similar to the SWE distribution (see Fig. 7). Blowing and drifting of snow occur most frequently (38–40 %) at wind exposed region, such as the higher elevated regions along the ridge. In the range of the isolated upstream ice bodies (including De Geerfonna) and the ice cap slopes snow erosion occurs of 30–34 %. Lower frequencies (20–24 %) are generally found in the forefield of the ice cap and on the south-eastern slope. These pattern imply that drifting snow events are triggered by the superposition of the paramount flow and katabatic winds, whereas the latter one is according to amount less efficient. This result is similar to observations of Grabiec et al. (2011), who found that air circulation patterns over Nordaustlandet and the mesoscale surface roughness play a major role in snow redistribution on the interior of Vestfonna. The magnitude of the modelled katabatic wind component along the slopes vary between 1–2 $m\,s^{-1}$ at 2 m height during the winter months, and thus leading to $u_* \leq 0.1\,m\,s{-}1$. The glacier wind components may be underestimated as a consequence of the assumption of homogeneous surface temperatures, which affects the buoyancy term and subsequently the occurrence of drifting snow events at the slopes.

Indeed it is observed, that katabatic glacier winds redistribute snow from the slopes to the ice edge forming a persistent surrounding snow band (see arrows in Fig. 6). Since the snow band exists all year, it is very likely that more accumulation takes place at these zones. Although katabatic winds might be underestimated, the distribution of the snow band along the Vestfonna margin and the nearby Backabreen and De Geerfona are clearly reproduced by the snowdrift model. Together with the radar-echo sounding (Figs. 2 and 6) it appears that after the 2–3 km wide snow band SWE decreases rapidly within a short distance of 2 km (marker B in Figs. 6 and 2). This

TCD
7, 709–741, 2013

decrease in SWE with altitude in the vicinity of the ice edge is also observed in most years by the snow pit measurements at location V2 and V4 (Möller et al., 2011b). The general spatial distribution along the slopes and the higher regions is reproduced by the model, as indicated by Fig. 2. Discrepancies are found in the region of the snow band and in the section between kilometer 54 and 58 along the radar-echo sounding path. The former one is most likely due to the limitations of the 250 m grid cell resolution in reproducing the complex small scale topography and its curvature pattern along the ice cap margin. Furthermore, the sudden change in mesoscale terrain roughness at the glacier fringe increases the turbulent kinetic energy and decreases the vertical wind shear. This process weakens the katabatic wind at the glacier slope, and thus the suspension capacity of the flow. Snow accumulated by this process is not captured by the model. To account for this process a Large Eddy Simulation model is required, rather than a Reynolds Averaged Models, in order to resolve the small scale flow pattern in detail. The overestimation of erosion between kilometer 54 and 58, however, can be probably attributed to boundary effects.

For the sake of clarity, drifting snow sublimation is discussed for the location VF-AWS, and has been integrated over the lower atmospheric boundary layer (10 m). Drifting and blowing snow sublimation shows a seasonal cycle with maximum values up to 8–12 % in April/May (see Fig. 8). During the winter months drifting snow sublimation rarely removes more than 6–8 % of the suspended snow. The seasonal variability can be attributed to the interplay between saturation deficit, temperature and wind speed. Particularly in spring conditions are favourable when high saturation deficits occur simultaneously with strong winds and moderate temperatures. The absorbed heat due to the sublimation process leads to a cooling and moistening of the near-surface airmass. As the moisture gradient decreases at the snow-atmosphere surface, surface sublimation gradually ceases. Since in the Arctic surface sublimation significantly contribute to the glacier surface mass balance, it is recommended to include drifting snow sublimation in such studies.

TCD
7, 709–741, 2013

8 Conclusions

This paper presents a high-resolution (250 m) spatial estimation of snowdrift over Vestfonna ice cap during the accumulation season 2008/2009. Blowing and drifting snow are frequent processes (10–25 %), which significantly modify snow accumulation distribution of the entire ice cap. In particular, along the wind exposed zones about 10–20 % of the primarily accumulated snow is redistributed to peripheral zones and must be considered a loss term for the ice cap mass balance. In this way, ice bodies such as the De Geerfonna receive up to 20 % additional snow mass. Based on the results, three characteric erosion zones can be identified on Vestfonna ice cap: (1) *inversion zone*, increase of SWE with altitude, (2) *precipitation zone*, decrease of SWE similar to the precipitation gradient and (3) *redistribution zone*, where the spatial distribution of snow is characterized by blowing and drifting of snow triggered by the paramount flow. These zones correspond to snow radar observations of Grabiec et al. (2011). Whether blowing snow from sea ice surfaces provide additional snow mass is still an open question. There is a pronounced variation in drifting and blowing snow sublimation during the simulation period with a maximum in April/May of 8–12 % and a minimum in winter with about 6–8 %. A detailed analysis of the effect of drifting snow sublimation on surface sublimation was not performed in this study, but will be covered in the future. Further work will also include drifting and blowing snow processes into the calculation of glacier mass balance and a more detailed description of snow pack processes.

Acknowledgements. This study was co-funded by grants no. BR 2105/6-1, SCHE 750/3-1 and SCHN 680/2-1 of the German Research Foundation (DFG). The Polish Ministry of Science and Higher Education funded the radar field work by grant no. IPY/279/2006. Additional funding was provided by the International SvalGlac-Project of the European Science Foundation through the German Federal Ministry of Education and Research (BMBF, grants no. 03F0623A and 03F0623B) and NCBiR/PolarCLIMATE-2009/2-1/2010. The authors acknowledge the logistical assistance of the Swedish Polar Research Secretariat in the field that was provided in the framework of the 3rd International Polar Year (IPY) core project “IPY Kinnvika” and of the Norsk Polar Institute for provision of logistical support at Oxford Halfoya field camp.

TCD
7, 709–741, 2013

References

Ahlmann, H.: Scientific results of the Swedish–Norwegian Artic Expedition in the summer of 1931, Part 8, Geogr. Ann., 15, 161–216, 1933. 711, 714

Anderson, R. and Haff, P.: Wind modification and bed response during saltation of sand in air, supplementum 1. Aoelian Grain Transport, 1: Mechanics, Acta Mech., 1, 21–52, 1991. 719

Beaudon, E., Arppe, L., Jonsell, U., Martma, T., Möller, M., Pohjola, V., Scherer, D., and Moore, J.: Spatial and temporal variability of net accumulation from shallow cores from Vestfonna ice cap (Nordaustlandet, Svalbard), Geogr. Ann., 93, 287–299, 2011. 711, 713

Bednorz, E. and Fortuniak, K.: The occurrence of coreless winters in central Spitsbergen and their synoptic conditions, Polar Res., 30, 12218, doi:10.3402/polar.v30i0.12218, 2011. 712

Beyers, J., Sundsbø, P., and Harms, T.: Numerical simulation of three-dimensional, transient snow drifting around a cube, J. Wind Eng. Ind. Aerod., 92, 725–747, 2004. 720

Bintanja, R.: The contribution of drifting snow sublimation to the surface mass balance of Antarctica, Ann. Glaciol., 27, 251–259, 1998. 711

Bintanja, R.: Snowdrift suspension and atmospheric turbulence, Part 1: Theoretical background and model description, Bound.-Lay. Meteorol., 95, 343–368, 2000. 714, 715, 716, 721

Boon, S., Burgess, D., Koerner, R., and Sharp, M.: Forty-seven years of research on the Devon Island ice cap, Arctic Canada, Arctic, 63, 13–29, 2010. 710

Braun, M., Pohjola, V., Pettersson, R., Möller, M., Finkelnburg, R., Falk, U., Scherer, D., and Schneider, C.: Changes of glacier frontal positions of Vestfonna (Nordaustlandet, Svalbard), Geogr. Ann., 93, 301–310, 2011. 712

Claremar, B., Obleitner, F., Reijmer, C., Pohjola, V., Waxegård, A., Karner, F., and Rutgersson, A.: Applying a mesoscale atmospheric model to Svalbard glaciers, Adv. Meteorol., 2012, 321649, doi:10.1155/2012/321649, 2012. 713, 723, 724

Crowe, C., Troutt, T., and Chung, J.: Numerical models for two-phase turbulent flows, Ann. Rev. Fluid Mech., 28, 11–43, 1996. 715

Durand, Y., Gyomarc'h, G., Mérindol, L., and Corripio, J.: Improvement of a numerical snow drift model and field validation, Cold Reg. Sci. Technol., 43, 93–103, 2005. 716

Elgobashi, S.: On predicting particle-laden turbulent flows, Appl. Sci. Res., 52, 309–329, 1994. 715

TCD
7, 709–741, 2013

Førland, E., Hanssen-Bauer, I., and Nordli, P.: Climate statistics and longterm series of temperature and precipitation at Svalbard and Jan Mayen, Det Norske Meteorologiske Institutt Klima Report, 21, 97, 1997. 712
Gauer, P.: Numerical modeling of blowing and drifting snow in Alpine terrain, J. Glaciol., 47, 97–110, 2001. 715, 716
Gore, R. and Crowe, C.: Effect of particle size on modulating turbulent intensity, Int. J. Multiphas. Flow, 15, 278–285, 1989. 715
Grabiec, M., Puczko, D., Budzik, T., and Gajek, G.: Snow distribution patterns on Svalbard glaciers derived from radio-echo soundings, Pol. Polar Res., 32, 393–421, 2011. 711, 713, 714, 724, 725, 727, 734, 738, 740
Hagen, J.: Glacier atlas of Svalbard and Jan Mayen, 129, Norsk polarinstitutt, 1993. 713
Hines, K. and Bromwich, D.: Development and testing of polar Weather Research and Forecasting (WRF) model, Part 1: Greenland ice sheet meteorology, Mon. Weather Rev., 136, 1971–1989, 2008. 723
Hines, K., Bromwich, D., Bai, L., Barlage, M., and Slater, A.: Development and testing of polar WRF, Part 3: Arctic land, J. Climate, 24, 26–48, 2011. 723
Jaedicke, C.: Snow drift losses from an Arctic catchment on Spitsbergen: an additional process in the water balance, Cold Reg. Sci. Technol., 34, 1–10, 2002. 711, 724
Käsmacher, O. and Schneider, C.: An objective circulation pattern classification for the region of Svalbard, Geogr. Ann. A, 93, 259–271, 2011. 712
Lehning, M., Löwe, H., Ryser, M., and Raderschall, N.: Inhomogeneous precipitation distribution and snow transport in steep terrain, Water Resour. Res., 44, W07404, doi:10.1029/2007WR006545, 2008. 714
Lenaerts, J. T. M., van den Broeke, M. R., Déry, S. J., König-Langlo, G., Ettema, J., and Munneke, P. K.: Modelling snowdrift sublimation on an Antarctic ice shelf, The Cryosphere, 4, 179–190, doi:10.5194/tc-4-179-2010, 2010. 711
Lenaerts, J. T. M., van den Broeke, M. R., van Angelen, J. H., van Meijgaard, E., and Déry, S. J.: Drifting snow climate of the Greenland ice sheet: a study with a regional climate model, The Cryosphere, 6, 891–899, doi:10.5194/tc-6-891-2012, 2012. 711
Liston, G. and Sturm, M.: A snow-transport model for complex terrain, J. Glaciol., 44, 498–516, 1998. 714, 716
Loeng, H.: Features of the physical oceanographic conditions of the Barents Sea, Polar Res., 10, 5–18, 1991. 712

TCD
7, 709–741, 2013

Maussion, F., Scherer, D., Finkelnburg, R., Richters, J., Yang, W., and Yao, T.: WRF simulation of a precipitation event over the Tibetan Plateau, China – an assessment using remote sensing and ground observations, Hydrol. Earth Syst. Sci., 15, 1795–1817, doi:10.5194/hess-15-1795-2011, 2011. 723

Mernild, S., Liston, G., Hasholt, B., and Knudsen, N.: Snow distribution and melt modeling for Mittivakkat Glacier, Ammassalik Island, southeast Greenland, J. Hydrometeorol., 7, 808–824, 2006. 710

Möller, M.: A minimal, statistical model for the surface albedo of Vestfonna ice cap, Svalbard, The Cryosphere, 6, 1049–1061, doi:10.5194/tc-6-1049-2012, 2012. 713

Möller, M., Finkelnburg, R., Braun, M., Hock, R., Jonsell, U., Pohjola, V., Scherer, D., and Schneider, C.: Climatic mass balance of Vestfonna ice cap, Svalbard: a spatially distributed assessment using ERA-Interim and MODIS data, J. Geophys. Res., 116, F03009, doi:10.1029/2010JF001905, 2011a. 713

Möller, M., Möller, R., Beaudon, E., Mattila, O.-P., Finkelnburg, R., Braun, M., Grabiec, M., Jonsell, U., Luks, B., Puczko, D., Scherer, D., and Schneider, C.: Snowpack characteristics of Vestfonna and DeGeerfonna (Nordaustlandet, Svalbard) – a spatiotemporal analysis based on multiyear snow-pit data, Geogr. Ann., 93, 273–285, 2011b. 711, 713, 714, 722, 724, 726

Möller, M., Finkelnburg, R., Braun, M., Scherer, D., and Schneider, C.: Variability of the climatic mass balance of Vestfonna ice cap (northeastern Svalbard), Ann. Glaciol., 54, 1979–2011, 2013. 713

Naaim, M., Naaim-Bouvet, F., and Martinez, H.: Numerical simulation of drifting snow: erosion and deposition models, Ann. Glaciol., 26, 191–196, 1998. 716, 720, 721

Pomeroy, J. and Gray, D.: Saltation of snow, Water Resour. Res., 26, 1583–1594, 1990. 716, 719, 722

Pomeroy, J. and Gray, D.: Snowcover accumulation, relocation and management., B. Int. Soc. Soil Sci., 88, 422–423, doi:10.1080/02626669609491514, 1995. 721

Pomeroy, J. and Male, D.: Steady-state suspension of snow, J. Hydrol., 136, 275–301, 1992. 720, 722

Pomeroy, J., Gray, D., and Landine, P.: The prairie blowing snow model: characteristics, validation, operation, J. Hydrol., 144, 165–192, 1993. 721

Rogers, A., Bromwich, D., Sinclair, E., and Cullather, R.: The atmospheric hydrologic cycle over the Arctic Basin from reanalyses, Part 2: Interannual variability, J. Climate, 14, 2414–2429, 2001. 713

TCD
7, 709–741, 2013

Schmidt, R.: Sublimation of Wind-Transported Snow: a Model, Rocky Mountain Forest and Range Experiment Station, Forest Service, US Department of Agriculture, 1972. 721
Schmidt, R.: Sublimation of snow intercepted by an artificial conifer, Agr. Forest Meteorol., 54, 1–27, 1991. 721
Schneiderbauer, S., Tschachler, T., Fischbacher, J., Hinterberger, W., and Fischer, P.: Computational fluid dynamic (CFD) simulation of snowdrift in alpine environments, including a local weather model, for operational avalanche warning, Ann. Glaciol., 48, 150–158, 2008. 715, 716
Schytt, V.: Scientific results of the Swedish glaciological expedition to Nordaustlandet, Spitsbergen, Geogr. Ann., 46, 242–281, 1964. 711
Skeie, P.: Meridional flow variability over the Nordic seas in the, Geophys. Res. Lett., 27, 2569–2572, 2000. 712
Stull, R.: An Introduction to Boundary Layer Meteorology, vol. 13, Springer, Kluver Academic, Dordrecht, the Netherlands, 1988. 717, 723
Svendsen, H., Beszczynska-Møller, A., Hagen, J., Lefauconnier, B., Tverberg, V., Gerland, S., Ørbæk, J., Bischof, K., Papucci, C., Zajaczkowski, M., Azzolini, R., Bruland, O., Wiencke, C., Winther, J.-G., and Dallmann, W.: The physical environment of Kongsfjorden-Krossfjorden, an Arctic fjord system in Svalbard, Polar Res., 21, 133–166, 2002. 712
Taurisano, A., Schuler, T., Hagen, J., Eiken, T., Loe, E., Melvold, K., and Kohler, J.: The distribution of snow accumulation across the Austfonna ice cap, Svalbard: direct measurements and modelling, Polar Res., 26, 7–13, 2007. 711, 712
Walczowski, W. and Piechura, J.: Influence of the West Spitsbergen Current on the local climate, Int. J. Climatol., 31, 1088–1093, 2011. 712

TCD
7, 709–741, 2013

Table 1. Notation.

u_*	friction velocity [$m\,s^{-1}$]
τ_0	surface shear stress [$kg\,m^{-1}\,s^{-2}$]
z	height above surface [m]
κ	von Kármán constant
ϕ_s	snow mass in saltation layer [$kg\,m^{-3}$]
ϕ_{max}	max. particle concentration (steady-state) [$kg\,m^{-3}$]
β	coefficient of expansion [K^{-1}]
θ	potential temperature [K]
K_M	eddy diffusivity [$m^2\,s$]
κ_{eff}	heat transfer coefficient [$m^2\,s$]
ν	kinematic viscosity [$m^2\,s$]
ν_t	turbulent viscosity [$m^2\,s$]
δ_{ij}	Kronecker delta
ρ	air density [$kg\,m^{-3}$]
k	turbulent kinetic energy [$m^2\,s^{-2}$]
ω	turbulent dissipation [s^{-1}]
α	$k-\omega$ model coefficient
β_k, β_k^*	$k-\omega$ model coefficients
$\sigma_k^*, \sigma_\omega^*$	$k-\omega$ model coefficients
ρ_s	snow density [$kg\,m^{-3}$]
e_{salt}	efficiency of saltation [$0 \le e_{salt} \le 1$]
h_{salt}	saltation layer height [m]
g	gravity acceleration [$m\,s^{-2}$]
u_{salt}	horizontal saltation particle velocity [$m\,s^{-1}$]
V	mean particle settling velocity [$m\,s^{-1}$]
u_{th}	friction velocity threshold [$m\,s^{-1}$]
q_e	erosion flux [$kg\,m^{-2}\,s^{-1}$]
q_d	vertical turbulent diffusion flux [$kg\,m^{-2}\,s^{-1}$]
q_s	horizontal flux in saltation layer [$kg\,m^{-2}\,s^{-1}$]
q_{salt}	snow mass flux in the saltation layer [$kg\,m^{-2}\,s^{-1}$]
ψ_s, ψ_t	sublimation-loss-rate coefficients [–]

TCD
7, 709–741, 2013

Table 2. Model parameters.

Parameter	Symbol	Value	Unit
Erosion efficiency	e_{salt}	5×10^{-4}	–
Fallout velocity	V	0.02	$m\,s^{-1}$
Fresh snow density	ρ_s	250	$kg\,m^{-3}$

TCD
7, 709–741, 2013

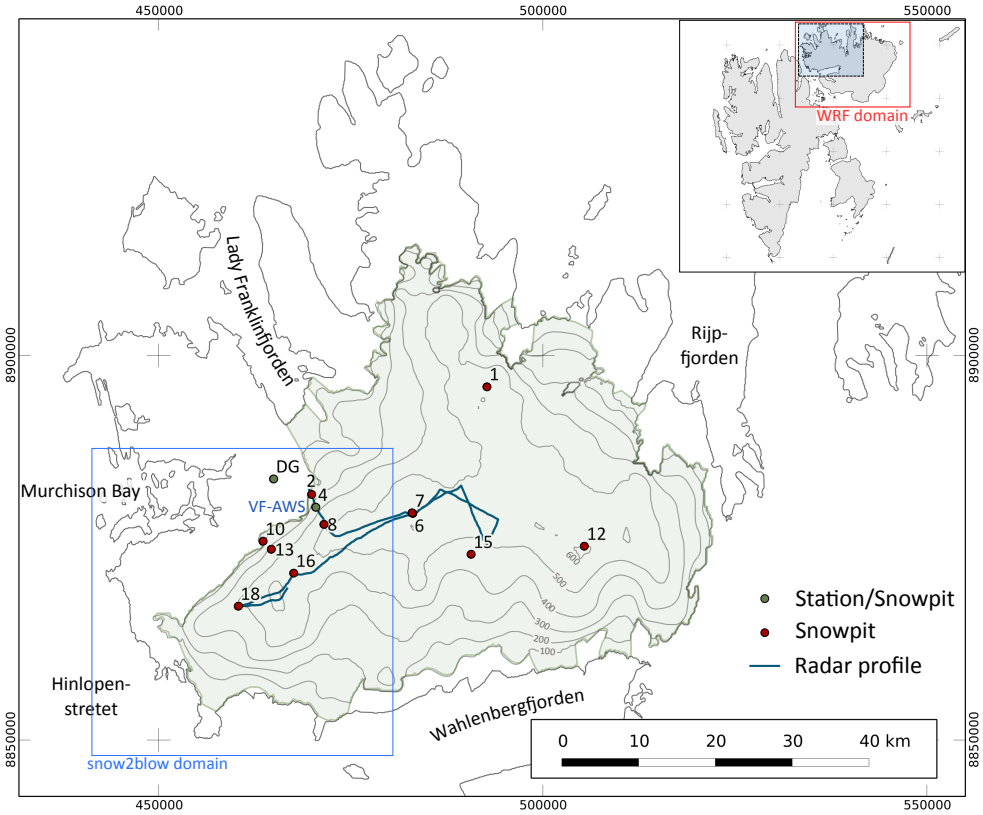

Fig. 1. Detailed map of Vestfonna ice cap (UTM 34N, WGS84). The grey shading shows the approximately edge of the ice cap. The locations of the Automatic Weather Stations VF-AWS (accompanied by snowpit measurement) are denoted as green dots, single snowpit measurements as red dots. The radio-echo sounding profile of Grabiec et al. (2011) is indicated as a blue line.

TCD
7, 709–741, 2013

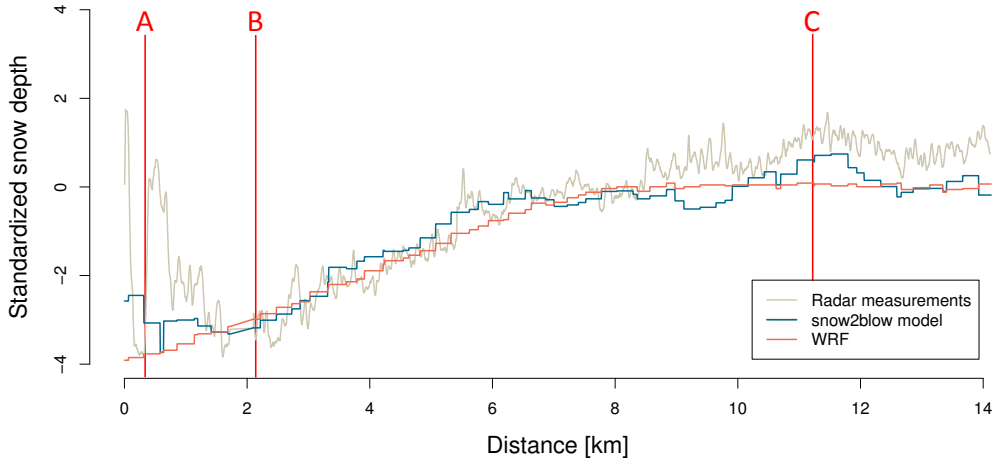

Fig. 2. The standardized anomalies (by subtracting the sample mean, and dividing by the sample standard deviation) of the radio-echo sounding, modelled snow depths and WRF along the profile shown in Fig. 1. Capital letters correspond to the markers given in Fig. 6.

TCD
7, 709–741, 2013

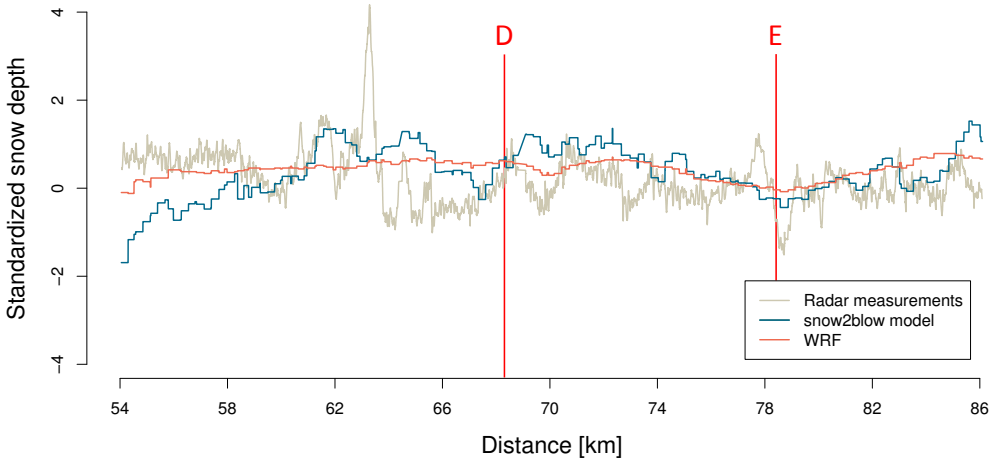

Fig. 3. The standardized anomalies (by subtracting the sample mean, and dividing by the sample standard deviation) of the radio-echo sounding, modelled snow depths and WRF along the profile shown in Fig. 1. Note that the mean SWE of the radio-sounding, snow2blow model and WRF model is approximately 0.34 m, 0.47 m and 0.56 m. Capital letters correspond to the markers given in Fig. 6.

TCD
7, 709–741, 2013

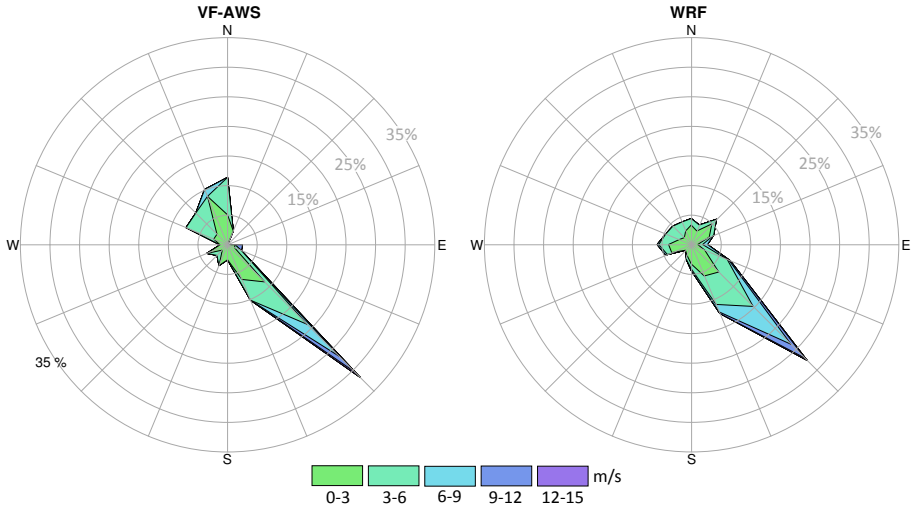

Fig. 4. Wind direction and speed measured at the VF-AWS (left) and modelled by the WRF (right).

TCD
7, 709–741, 2013

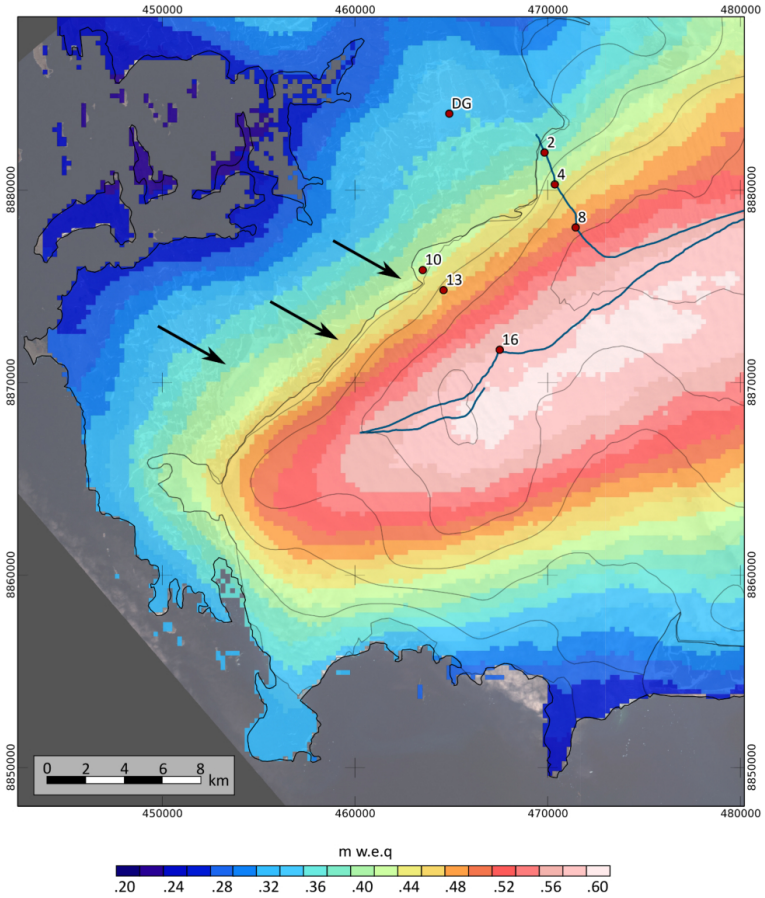

Fig. 5. Snow accumulation in m w.e. from the WRF model runs over the period September 2008 to May 2009. The arrows mask regions of special interest which are discussed in detail in the text. The blue line shows the radio-echo sounding profile of Grabiec et al. (2011) in May 2009.

TCD
7, 709–741, 2013

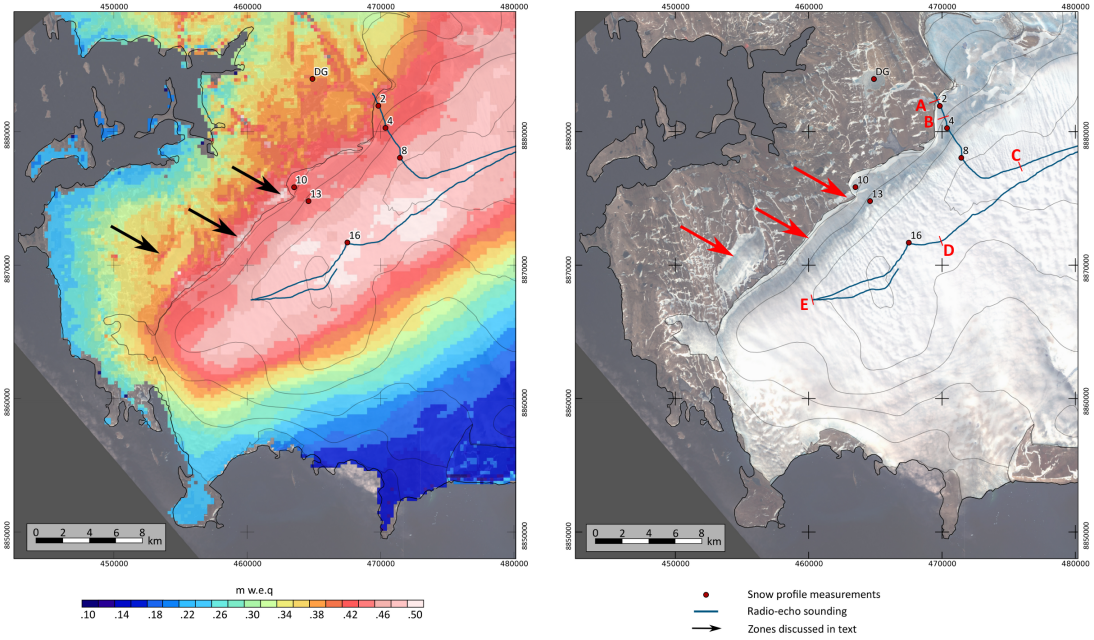

Fig. 6. Modelled snow depths in m w.e. after the accumulation season 2008/2009 (left) and ASTER satellite image from 17 August 2000 (right, UTM 34N, WGS84). The arrows mark regions of special interest which are discussed in detail in the text. The blue line shows the path of the radio-echo sounding measurements in May 2009.

TCD
7, 709–741, 2013

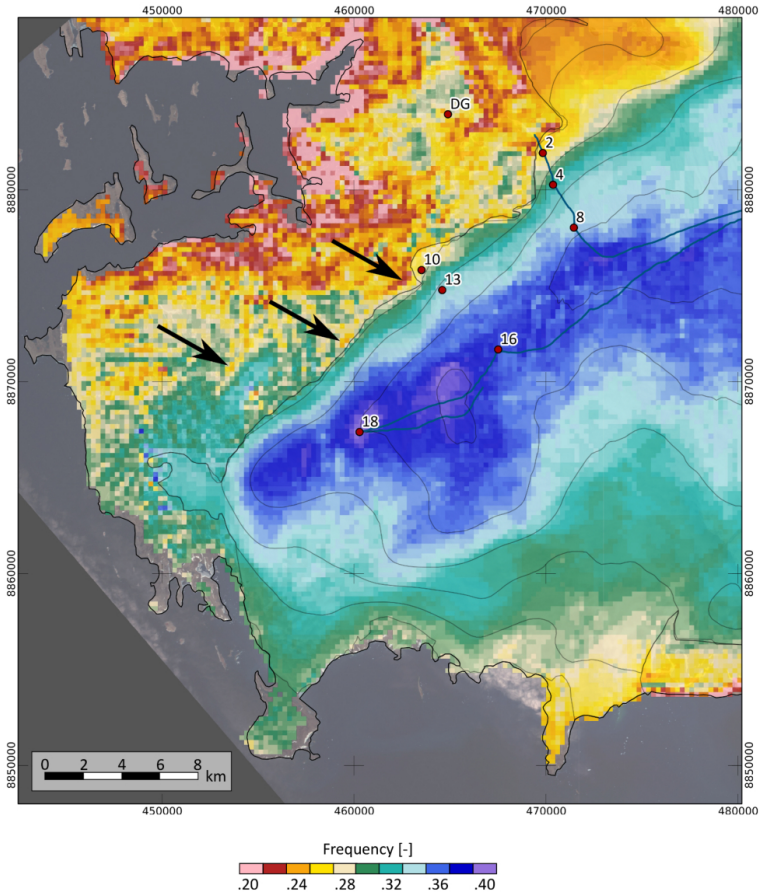

Fig. 7. Drifting snow frequency in the period September 2008 to May 2009, defined as the ratio of days with non-zero erosion flux and the total number of days. The blue line shows the radio-echo sounding profile of Grabiec et al. (2011) in May 2009.

TCD
7, 709–741, 2013

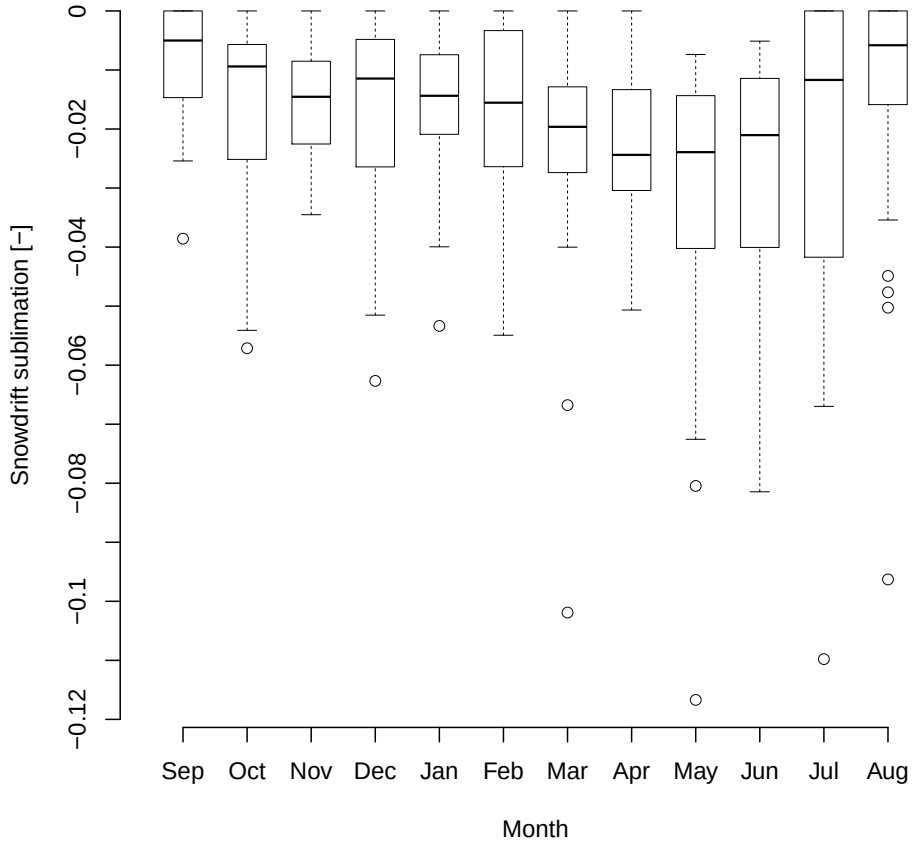

Fig. 8. Interseasonal variability of the mean drifting snow sublimation within the near-surface layer (below 10 m) at the location VF-AWS. The boxes spread between lower and upper quartiles of the values with the median shown as the thick line in between, the whiskers extend the boxes by 1.5 times the inter quartile range. Values outside this range are considered as outliers.

TCD
7, 709–741, 2013